Production of $CaCO_3$/hyperbranched polyglycidol hybrid films using spray-coating technique

Kalina Malinova [a], Manfred Gunesch [b], Sabrina Montero Pancera [c], Robert Wengeler [d], Bernhard Rieger [b], Dirk Volkmer [a]

[a] *Augsburg University, Chair of Solid State and Materials Chemistry, Institute of Physics, Universitaetsstrasse 1, D-86159 Augsburg, Germany*
[b] *WACKER Chair of Macromolecular Chemistry, Technical University of Munich (TUM), Lichtenbergstrasse 4, D-85747 Garching bei Munich, Germany*
[c] *BASF SE, G-CAE/NA – Lu-Klebs-u. Hartm. H, 67056 Ludwigshafen, Germany*
[d] *BASF SE, GCT/T – L540, 67056 Ludwigshafen, Germany*

1. Introduction

Biomineralizing organisms produce scales, shells or skeletons that are hybrid materials, composed of inorganic components such as calcium carbonate or phosphate and a (minor) organic part consisting of acidic macromolecules that display a high content of carboxylate, phosphate or sulfate groups [1,2]. These biominerals often possess unique crystal textures that give rise to unusual mechanical and optical properties such as strongly increased toughness, impact resistance and characteristic luster [3,4]. By using nanoindentation, it was demonstrated that calcite semi-nacre ($H \sim 3$–6 GPa; $E = 60$–120 GPa) and pure calcite ($H \sim 2$–3 GPa) are harder and stiffer than calcite fibers ($H \sim 0$–3 GPa; $E = 20$–80 GPa). Rhynchonelliform brachiopods, for instance, have a three-layered shell, where the secondary layer is composed of calcite fibers [5]. Many scientists were intrigued by the hierarchical order and structure of biominerals [6] leading to excellent mechanical properties [7], which provide a source of inspiration for the fabrication of novel organic–inorganic composites. From the perspective of producing materials reminiscent of biominerals (e.g., nacre) at large scale, two technological aspects deserve further attention: First, to implement biomimetic production strategies requires vast conceptual simplifications of the putative mechanism(s) by which biominerals are formed and thus the value of a production strategy has to be assessed by screening gross morphological features of the as-synthesized composite materials. This more or less descriptive (yet fast) step might then be augmented by more sophisticated analyses of

Abbreviations: SAM, self-assembled monolayer; ACC, amorphous calcium carbonate; LBL, layer-by-layer; LFS, liquid-feed solution; M_n, number average molecular weight; *hb*-PG, hyperbranched polyglycidol; *hb*, hyperbranched; COO-terminated *hb*-PG, hyperbranched polyglycidol carboxylates (carboxylate functionalized *hb*-PG); OPO_3HPhOH-terminated *hb*-PG, hyperbranched polyglycidol phosphates (phosphate monoester functionalized *hb*-PG); SO_4-terminated *hb*-PG, hyperbranched polyglycidol sulfates (sulfate functionalized *hb*-PG); DHBCs, double-hydrophilic block copolymers; $CaCO_3$, calcium carbonate; at.%, atomic concentration; E_R, reduced Young's modulus; PAANa, poly(acrylic acid) sodium salt.

mechanical properties, which constitutes a limiting factor in terms of time and equipment required to obtain meaningful results. Second, genetic control over biomineral production has to be replaced by simple self-assembly approaches. For the latter, it is anticipated that finding appropriate synthetic models of biomacromolecules occluded within biominerals might pave the way toward hierarchical materials that exhibit superior mechanical performance. It should be noted in this context, however, that even a seemingly simplistic task such as selective formation of artificial aragonite platelets that bear morphological features closely related to the brick-and-mortar arrangement of tabular aragonite crystals found in nacre has remained elusive so far, despite partial success reported by several groups [8–12].

In the realm of $CaCO_3$/polymer composites, many studies have shown that numerous experimental parameters, including pH [13], temperature [14], foreign ions [15], chemical nature of the organic additives [9,15] and templates (matrices such as chitin, cellulose or chitosan) [9] affect the $CaCO_3$ crystal phase and the resulting crystal morphology. DHBCs polymers demonstrated remarkable effects in crystallization for a wide range of inorganic and inorganic–organic hybrids [13,15,16]. Other classes of polymers such as dendrimers were also discovered as active additives for controlled $CaCO_3$ precipitation [17]. Hyperbranched polymers belong to these synthetic tree-like macromolecules class and furthermore, they are also accepted to be polysaccharide and polyethylene glycol analogues due to their good water-solubility and biocompatibility [18–20]. Due to their unique properties, easy one-pot synthesis, low cost production and well-defined architecture with the possibility to attach different reactive terminal groups in a straight-forward manner, hyperbranched polymers have a wide range of industrial and biomedical applications [21]. Hyperbranched materials also have outstanding mechanical properties such as tensile strength and compressive modulus which reflect the compact highly branched structures [22]. The application of hyperbranched polymers is largely unexplored in $CaCO_3$ mineralization processes. Only few reports [20,23–25] as yet appeared in the literature where functionalized hyperbranched polymers possessing carboxylate or sulfate groups were employed as additives for the growth of isolated $CaCO_3$ crystals. To the best of our knowledge, hyperbranched polyglycidols bearing phosphate monoester end groups as well as their influence on $CaCO_3$ crystallization are unknown until now. As outlined above, the appropriate selection of both the synthetic polymers and a scalable production method is of major importance for producing hybrid thin films. Numerous established laboratory (i.e., small scale) techniques exist for the fabrication of $CaCO_3$ thin films (carbonate diffusion in different variants [26], self-assembled monolayers (SAMs) [23], layer-by-layer (LBL) [10], Langmuir monolayer [27], electrophoretic deposition [11], are known, as well as continuous flow deposition techniques [12]. Each of these techniques suffers from specific disadvantages: Most of them are time consuming, pH dependent, and none of them can be applied using high concentrations, thus resulting in low deposition rates [28]. Therefore, there is a demand for improved methods in order to cover large surface areas with dense composite thin films in a production efficient and economically viable fashion.

We here present a novel strategy to obtain nanostructured composites of $CaCO_3$ by using spray-coating technique in a combination with functionalized hyperbranched low molecular weight polyglycidols. For the preparation of calcium carbonate composites, the spray-coating technique offers many advantages as compared to conventional deposition techniques, such as (1) simple, fast and easy to handle spraying process; (2) no need to apply pre-coatings; (3) easy scale-up due to the usage of simple and industrially established equipment; (4) the possibility to cover large areas and (5) to apply highly concentrated solutions, resulting in deposition rates superior to that of all other methods. In this work, we focus on the preparation of low molecular weight hyperbranched polyglycidols bearing different functional groups and effects of these on the formation of calcium carbonate composites prepared via spray coating. Attractive targets for these $CaCO_3$/polymer composites might include traditional wall paintings, coatings of transportation systems such as ships or off-shore buildings, coatings of medical devices (i.e., tubings, syringes or pumps), ceramics, as well as biocompatible biomaterials such as bone or dental implants [29].

2. Materials and methods

$CaCl_2 \times 2H_2O$ and Na_2CO_3 were purchased from Merck. These chemicals were used as received without further purification. High-purity 18.2 MΩ cm double-demineralized water was used as solvent for all solutions. Microscopy glass slides (ca. 76 × 26 mm; Menzel-Gläser) were used as test substrates in spray coating procedures leading to calcium carbonate composites.

The deposited calcium carbonate composites were characterized with the following techniques: Thermogravimetric analysis (TGA) was performed with a TGA/SDTA851 Mettler Toledo analyzer in a temperature range of 25–1100 °C in flowing nitrogen at a heating rate of 5 °C min^{-1}. Scanning electron microscope (SEM) images were recorded using a Zeiss DSM 962 scanning electron microscope. Energy dispersive X-ray analysis (EDX) was performed on an EDAX (Phönix) X-ray detection system with 30 mm^2 SUTW window. Fourier transform infrared (FTIR) spectra were recorded from KBr pellets in the range 4000–400 cm^{-1} on a Bruker IFS FT-IR spectrometer. X-ray powder diffraction (XRPD) patterns were measured using Philips PANalytical X'Pert PRO diffractometer with Cu Kα-radiation (Philips PW 3373, 45 kV, 40 mA) between 5° and 80° (2Θ) with a step-size of 0.0334° (2Θ) and a sample time of 10 s/step. The refinement process was performed by using the Jana2000 Program. Raman spectroscopy was performed with a Jobin Yvon Horiba Raman spectrometer equipped with a He–Ne-laser at a wavelength of 633 nm. Thickness profile measurements were performed with a Dektak 150 profilometer from Veeco (stylus diamond tip with radii 2.5 μm). X-ray photoelectron spectroscopy (XPS) measurements were performed by a Physical Electronics 5800 Multitechnique ESCA System using monochromatic Al Kα radiation (1486.6 eV) X-ray source operated at 250 W (13 kV and 19 mA). The photoelectrons were analyzed using a spherical capacitor analyzer (Phi Model 10-360). The pressure in the sample analysis chamber was 4×10^{-9} Torr. Survey scans (187.85 eV pass energy, 0.4 eV step size), and high-resolution XPS spectra (23.35 eV pass energy, 0.125 eV step size) were acquired to determine surface compositions. The spot size was 800 × 800 μm at normal incidence to the sample. Physical Electronics *MULTIPAK V6.1A* software was applied to deconvolute XPS spectra. XPS analysis was taken at a take-off angle of 45°, and the binding energy was calibrated by setting the C(1s) peak of hydrocarbons to 284.8 eV. For all cases studied, XPS analysis indicated the presence of S(2p), Ca(2p), O(1s) and C(1s) peaks. An Olympus IX70 inverted stage microscope was used to capture optical micrographs and polarization optical micrographs of polycrystalline thin films mounted between crossed polarizers. Mechanical properties were measured by using a Nanotest™ 600 by Micro Materials Ltd., Wrexham (UK), which is a pendulum-based nanoindenter (i.e., samples are mounted vertically). A Berkovich pyramidal diamond tip was used for all indentation measurements, penetrating into the specimen surface at a controlled loading rate of 7.5 mN. The load–displacement curves for each sample were performed at a depth until 500 nm. The nanoindentation instrument uses Nano-Test Platform software, which employs Oliver–Pharr data analysis

method to obtain the hardness [30]. As reference sample, natural calcite was indented parallel to the freshly cleaved rhombohedral (1 0 1) cleavage plane. For the purpose of statistical reliability, 45 indents for calcite and one hundred for the calcite composites were made to obtain statistically averaged results.

2.1. Experimental set-up for spray coating deposition of $CaCO_3$ composites

$CaCO_3$ composites were prepared from two aqueous liquid-feed solutions (LFSs) as starting materials. Liquid-feed solution 1 (LFS 1) consists of an aqueous Na_2CO_3 solution mixed under vigorous stirring for 40 min with functionalized hyperbranched polyglycidol (*hb*-PG). The functionalized hyperbranched polyglycidols (*hb*-PGs) were added to the Na_2CO_3 solutions prior to mixing, because at a high pH value (in our experiments pH = 11.2) the different anionic groups are completely deprotonated. Therefore, the negative anionic charges are compensated by sodium cations. When a $CaCl_2$ solution is mixed with *hb*-PGs, sol–gel phase separation occurs due to the sequestration of Ca^{2+} ions bridging the anionic groups which is accompanied by hydrophobic interactions between the organic branches of the *hb*-PGs. Three different hyperbranched polyglycidols were used: sulfate functionalized *hb*-PG (SO_4-terminated *hb*-PG), carboxylate functionalized *hb*-PG (COO-terminated *hb*-PG) and phosphate monoester functionalized *hb*-PG (OPO_3HPhOH-terminated *hb*-PG). For synthesis, derivatization and discussion of hyperbranched polyglycidols, see the Supplementary Material. In a typical procedure, SO_4-terminated *hb*-PG (3.7 mg/mL), or COO-terminated *hb*-PG (4.65 mg/mL), or OPO_3HPhOH-terminated *hb*-PG (10 mg/mL at the first experiment and 1.23 mg/mL in the second experiment) was dissolved in an aqueous solution of Na_2CO_3 (100 mL, 0.5 M). The total final concentration of functional groups employed from each polymer was approx. 0.02 M (sum over all functionalized monomer units stemming from the polyglycidol and 0.0025 M (for the second experiment performed in the presence of OPO_3HPhOH-terminated *hb*-PG). Liquid-feed solution 2 (LFS 2) consists of an aqueous $CaCl_2$ solution (100 mL, 0.5 M). The resulting molar ratio was thus: functional group/Ca^{2+}/CO_3^{2-} = 1/25/25. The resulting pH values for LFS1 and LFS2 were 11.2 and 5.7, respectively. The spray-coating experimental set-up consists of a peristaltic pump, manometer and nozzle (detailed description of the spray coating procedure, conditions and a technical drawing are given in the Supplementary Material, Fig. S1). All experiments were repeated at least twice. Control experiments were also carried out employing an identical experimental set-up either in absence of polyglycidol or with unmodified polyglycidol.

3. Results and discussion

3.1. Spray-coating preparation of vaterite composites in the presence of SO_4-terminated hb-PG

Different kinds of macromolecules have been tested for the formation of $CaCO_3$–organic composite thin films [15]. In contrast to the frequent usage of sulfonate-based polymers, few reports have previously considered sulfate-based polymers (whether being synthetic [16,20,24] or natural [9,31]) as effective modifiers for calcium carbonate crystallization. Vaterite stabilization in bulk over long periods of time [13,32,33] and formation of continuous pure vaterite thin films [34] in the presence of different polymers have been achieved by several groups. To the best of our knowledge, there is only a single publication [24] that describes functionalized hyperbranched polyesters possessing sulfonic acid groups and their influence on the formation of single-phase, spherical vaterite particles with a narrow size distribution and rough surface. Herein, we present the preparation of a dense vaterite thin film obtained by spray-coating employing a SO_4-terminated *hb*-PG solution at a concentration of 0.02 mol/L. The initial precipitation of an amorphous calcium carbonate (ACC) thin film was verified by optical microscopy and Raman spectroscopy. The amorphous phase consists of close packed contiguous colloid particles with apparently no associated birefringence (Fig. S10c, Supplementary Material). The Raman spectrum only showed a single carbonate vibration at 1079 cm^{-1} and a broad hump below 300 cm^{-1} confirming that the obtained product is ACC (Fig. S10a, Supplementary Material) [35]. However, a complete transition from the ACC precursor into polycrystalline thin film was readily achieved by heating the sample at 70 °C for 30 min. According to XRPD measurements, this yields an optically birefringent hybrid thin film (Fig. S10d, Supplementary Material), which contains pure vaterite. In addition, when using spray technique for the preparation of $CaCO_3$ composite coatings in combination with functionalized hyperbranched polyglycidols bearing phosphate monoester, sulfate and carboxylate groups, the thus-prepared $CaCO_3$ composite thin films did cover the substrate surface completely. Polarization optical micrographs of polycrystalline thin films, taken at low magnification, are shown in Fig. S10 (Supplementary Material). To evaluate the influence (if any) of the functionalized polymer on the formation of dense composite thin films, we used the spray technique either in the absence of any organic additives or in the presence of non-functionalized hyperbranched polyglycidol (under otherwise identical conditions). In both cases, only isolated calcite crystals showing the typical rhombohedral form were observed. No dense $CaCO_3$ polycrystalline thin films were obtained (Figs. S11 and S12, Supplementary Material). The XRD pattern in both cases indicated formation of pure calcite. These results clearly indicate that there is a strong interaction between the different functional groups (phosphate monoester, sulfate and carboxylate groups) and calcium ions that served as a reaction depot for the formation of dense $CaCO_3$ polycrystalline thin films.

Phase purity of the composites was confirmed by comparing the experimental X-ray powder diffraction (XRPD) patterns to reference diffraction data taken from the PDF-4 + database [36].

Fig. 1 shows the XRPD patterns of the deposited $CaCO_3$ composite obtained in the presence of SO_4-terminated *hb*-PG, which exclusively leads to the formation of vaterite. It should be noticed that the annealed films show an exceptional long-term stability (Fig. 1).

As a crystal model for the Rietveld refinement of the vaterite phase, the crystal structure of vaterite with the unit cell parameters and space group closest to the measured data for the vaterite thin film was applied (initial coordinates and displacement parameters taken from ISCD, Ref. No. 15879) [37]. When applying the March-Dollas formula [38], different directions of preferred orientation were tested. The best solution was obtained in case of preferred orientation chosen along the [0 0 1] direction. The final Rietveld plots are presented in Fig. S13 (Supplementary Material).

In contact with aqueous solution, vaterite normally transforms rapidly into thermodynamically more stable calcite within hours via a dissolution–recrystallization process [39]. It is assumed that the stabilization of vaterite in liquid solution can be denoted due to preferential adsorption of the organic additives (AOT [33] and DHBC [13]) on the vaterite surface. Here, we report a stable vaterite composite obtained in high purity after annealing at 70 °C. It seems surprising that within 9 months the synthesized vaterite/SO_4-terminated *hb*-PG composite does not show any sign of phase transformation, as can be clearly seen in the series of XRPD patterns displayed in Fig. 1. To the best of our knowledge, this is the first example that describes a successful stabilization of a spray-coating vaterite composite in the presence of SO_4-terminated *hb*-PG over such a long period of time. The polymorphism of the film was also characterized by Raman and FT-IR spectroscopy (Figs. S14 and S15,

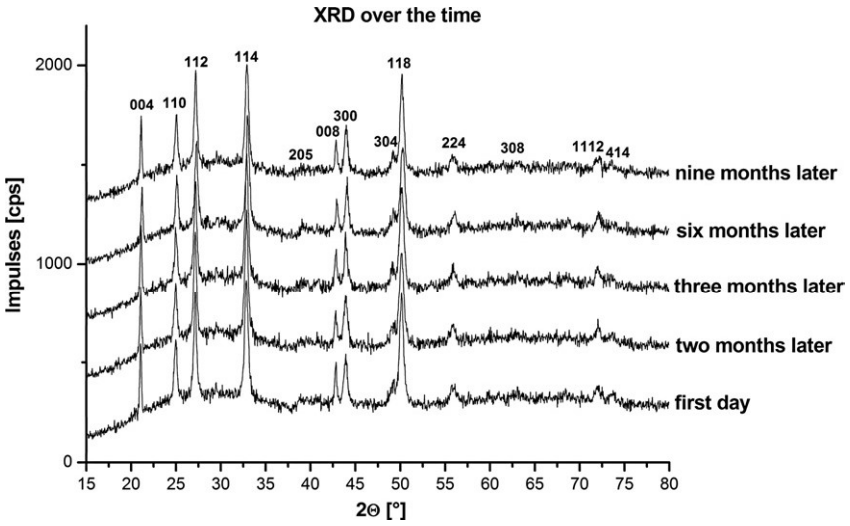

Fig. 1. Change of X-ray diffraction patterns over time of a vaterite composite thin film prepared by spray-coating technique in the presence of SO_4-terminated *hb*-PG.

Supplementary Material). Both spectra clearly identifies vaterite as crystalline phase from the characteristic peaks at 745 cm^{-1} (v_4) and at 1092 cm^{-1} (v_1). The infrared data display four additional absorption bands that correspond to the sulfate groups and the C–H stretching modes arising from the polymer (Fig. S15, Supplementary Material). The presence of three bands (1049, 1122 and 1255 cm^{-1}) in the spectrum can be explained with a C_{2v} symmetry for SO_4^{2-} groups stemming from the polymer. As a result, the (v_{as}) region for the sulfate group is strongly split into three bands due to a triply degenerated asymmetric mode (v_3) [40]. The band at 2930 cm^{-1} can be ascribed to the C–H stretching mode. Fig. 2 shows the typical scanning electron microscopy (SEM) images of the vaterite composite. The composite consists of polycrystalline spherical aggregates typical for vaterite (Fig. 2a), which are built up of small needle-type nanoparticles with a size of 40–50 nm.

The aggregates show coalescence giving rise to a thick coating, which possesses a pronounced roughness. This morphology is typical for strong interactions between crystallizing $CaCO_3$ and functional anionic groups which effectively suppress crystal growth [13]. SEM images taken at higher magnification (Fig. 2b) show that the aggregates within the polycrystalline vaterite thin film have an external texture built from uniform nanoparticles. The average size of these vaterite subunits was determined to be about 40–50 nm by comparing the profile width of a standard profile with a sample profile according to the Debye–Scherrer formula [41]. The average size of single crystal domains thus obtained (40–50 nm) is almost identical to the characteristic size of the vaterite primary particles measured from the SEM micrographs (approximately 60 nm). Thus, it can be concluded that the vaterite spherulites are composed of needle-shaped single crystals that are radially orientated. The average thickness of the vaterite coating is about 4–7 μm according to profilometer measurements, which corresponds to 1–2 times of the av. diameter of the aggregates.

The amount of SO_4-terminated *hb*-PG adsorbed on the obtained polycrystalline vaterite aggregates was determined by TGA (Fig. S16, Supplementary Material). Two weight loss regimes were observed as the film was heated from 25 to 900 °C: 41.96 wt.% above 700 °C, which is due to decomposition into CO_2 and CaO and weight loss of 3.22 wt.% between 150 and 300 °C, which is due to the decomposition of the *hb* oligomers. The pure SO_4-terminated *hb*-PG itself has a weight loss of 44.1 wt.% in the same temperature region of 150–300 °C. Thus, the composite contains between 4.6 wt.% and 7.3 wt.% of polymer (calculated from the difference between measured and theoretical weight loss of both $CaCO_3$ and the polymer). The assignment of the decomposition steps was accomplished by comparison with the TGAs of pure $CaCO_3$ and SO_4-terminated *hb*-PG (Figs. S16 and S17, Supplementary Material). Wang et al. [24] reported an amount of 7.9 wt.% of sulfonic-based hyperbranched polymers that is bound to vaterite crystals resulting from direct mixing of stock solutions. Via slow CO_2 gas diffusion as well as using a sulfate-based *hb*-polymer [20], pure calcite particles were produced, showing 5.3 wt.% of

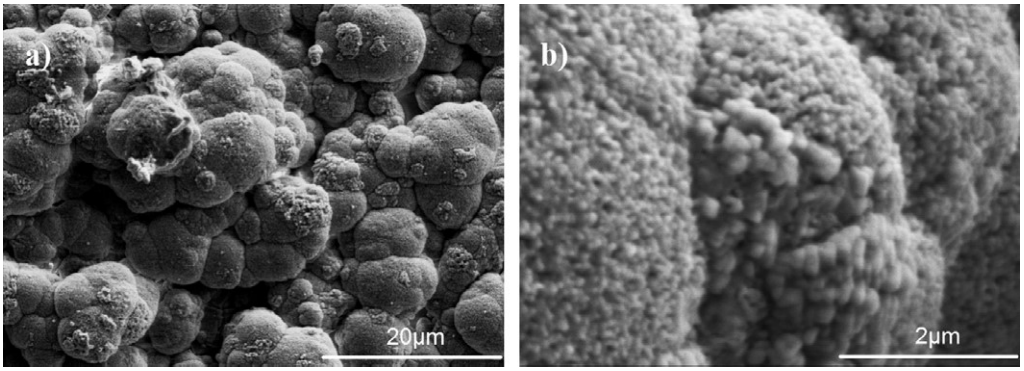

Fig. 2. SEM micrographs showing morphological characteristics of vaterite/SO_4-terminated *hb*-PG composite thin films formed via spray-coating technique. The micrographs were obtained from the film after annealing at 70 °C for 30 min: (a) low magnification and (b) high magnification.

adsorbed polymer. The generation of different polymorphs and the lower content of organic components reported in this study might attribute to the different crystallization methods.

Employing sulfated hyperbranched polymers similar to ours Meng and co-workers have reported on formation of pure vaterite when using likewise polymer concentration [24]. The fast precipitation (direct mixing of stock solutions), which occurs also in spray-coating experiments, seems to be essential for obtaining pure vaterite, in contrast to slow vapor diffusion experiments where pure calcite is formed, even at much higher polymer concentration [20]. The degree of functionalization of the polymer, on the other hand, seems only to have a minor role compared to the crystallization method. Vapor diffusion method [20] and fast precipitation [24] yielded pure calcite or vaterite polymorph, respectively, at nearly the same polymer degree of functionalization (approximately 60%).

3.2. XPS analysis of vaterite/SO_4-terminated hb-PG composite

The FT-IR spectrum recorded from samples of vaterite/SO_4-terminated *hb*-PG composites provide evidence for the presence of sulfate and C–H groups stemming from the polymer. This raises the question for the location of polymer in the composite and its putative interaction with the $CaCO_3$ particles. Accordingly, XPS analysis was employed to determine the concentration of polymer at the particle surface and to obtain concentration-depth profiles. The film surface was etched by sputtering with Ar^+ ions: the Ar^+ ion gun was used to slowly remove sample material (~1 nm/min) in a stepwise fashion. XPS measurements of non-etched ($t = 0$) and etched areas of vaterite/SO_4-terminated *hb*-PG composite at different times ($t = 1$, 10, 20, 30, 40, 50, 60, 70 and 80 min) were performed. The resulting fresh surface layers of the thin film were scanned periodically by XPS in order to determine the depth profile of the chemical composition.

The inset of Fig. 3 shows the detail spectra in the S(2p) binding energy range. The peak at 169.0 eV can be assigned to the S–O bonds in sulfate groups of the polymer [42]. The evaluation of the XPS data shows that the atomic concentration (at.%) of sulfur has the highest value of 0.45 at.% at the surface of the sample, before being etched by Ar^+ (Fig. 3a, $t = 0$ min). With increasing time of etching, the S concentration decreases and reaches the detection limit of the XPS instrument (~0.1 at.%) (Fig. 3a). These results further demonstrate that the S concentration decreases with increasing depth of the composite. Thus, we can conclude that the sulfur is predominantly located in the external region of the vaterite/SO_4-terminated *hb*-PG thin film. The total carbon concentration decreases with increasing etching times, whereas the Ca and O concentrations increase (Fig. 3b; Fig. S18 see Supplementary Material), which is in satisfying agreement with the conclusions drawn above.

As a conclusion from the XPS data, the topmost part of the vaterite surface and its vicinity are rich in polymer species (S, C from hydrocarbons), while the $CaCO_3$ content increases and finally dominates with increasing the penetration depth into the vaterite composite. XRPD data showed no differences in the unit-cell parameters when crystallized in the presence or absence of SO_4-terminated *hb*-PG, additionally indicating that the polymer was surface bound and not incorporated into the crystal lattice. Furthermore, it was shown that SO_4-terminated *hb*-PG is preferentially adsorbed on the exterior of the vaterite crystals, probably acting as a surface stabilizer. Thus, a surface-confined polymer layer is probably the reason for the observed unusual long-term stability of the vaterite composite. At an atomistic level, the stabilization of vaterite particles might be attributed to the branched structure of the polyglycidol backbone, but this interpretation would require support from additional experimental investigations.

Some authors [43] discussed that polymers having lower M_n values adsorb more efficiently on crystal surfaces than polymers with greater M_n. Since the synthesized functionalized hyperbranched oligomers used in this study have molecular weights (about $M_n = 700$–800 g/mol), they should be anchored relatively strongly at the surface of the aggregates. In this context, it can be rationalized as to why SO_4-terminated *hb*-PG stabilizes vaterite over a period of more than 9 months.

3.3. Spray-coating preparation of calcite–vaterite composites in the presence of COO-terminated hb-PG

As mentioned in the introduction, the organic macromolecules from the biominerals are typically rich of carboxylate groups. Thus, another biomimetic $CaCO_3$ composite was produced in the presence of hyperbranched polyglycidol functionalized with carboxylate groups (COO-terminated *hb*-PG). The XRPD diffractogram and quantitative phase analysis (Figs. S21 and S22, Supplementary Material) indicate that the composite is comprised of 50% calcite, 45% of vaterite and 5% of contamination with NaCl. A preferred orientation along the [0 0 1] direction for both calcite and vaterite was observed. The crystalline domain size of 102.7 nm for calcite determined from the (1 0 4) reflex and 51.1 nm for vaterite, determined from the (1 1 2) reflex, respectively, were calculated according to the Scherrer formula. The FT-IR and Raman spectra of the obtained composite also indicate the presence of both polymorphs (Figs. S23

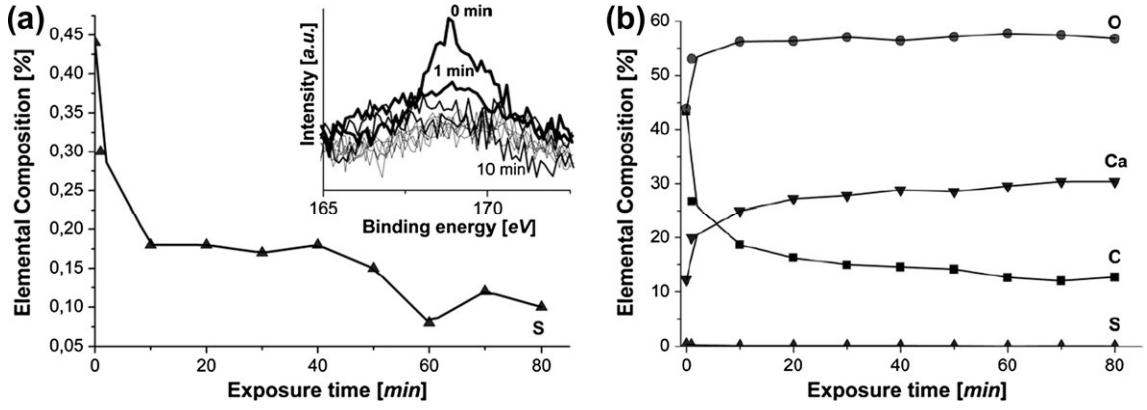

Fig. 3. Chemical composition (Ca, O, C, S) of vaterite/SO_4-terminated *hb*-PG coating derived from XPS spectra after increasing Ar^+ etching times (depth profile). (a) Significant decrease in the sulfur concentration, as derived from the detailed spectra in the S(2p) range (inset) and (b) the evolution of chemical composition (Ca, O, C, S) at the surface as a function of Ar^+ etching times.

and S24; detailed explanations of both spectra can be seen in the Supplementary Material). Typical SEM micrographs show that the $CaCO_3$ composite exhibits two different morphologies, typical for each polymorph (Fig. 4). Big, rough, spherulitic aggregates are found for vaterite, and a rhombohedral-lamella shaped structure corresponds to calcite (Fig. 4). The mechanically interlocked crystal aggregates associate with two types of crystal polymorphs found in the composite, which is promoted by the COO-terminated *hb*-PG, since no polycrystalline thin film formation was observed in the control experiment in absence of the polymer (Figs. S11 and S12, Supplementary Material). The surface of the composite is very rough, with an average thickness of about 2–4 μm as determined by the profilometer.

In addition to the control experiments performed, a $CaCO_3$ composite in the presence of PAANa (M_w = 2100 g/mol) was produced by spray-coating. Although experiments were done under the same conditions, PAANa did not exert the same strong influence on the morphology of $CaCO_3$ thin films when compared to COO-terminated *hb*-PG. Moreover, isolated crystal islands rather than a dense composite coating were observed (Fig. S10, Supplementary Material). Whereas linear polycarboxylates seem to act as an inhibitor for crystal nucleation, the hyperbranched polymers employed in the current study are more efficient crystal habit modifiers. Therefore, the specific $CaCO_3$ composite structure and morphology is, beside the functional group of the polymer, dominated by the structure of the polymer. Composite films thus prepared possess a typical average thickness of about 0.5–0.7 μm, as determined by AFM. TGA analysis was used to determine the amount of organic content within the film, showing weight loss of 35.32 wt.% above 600 °C, which attributes to the decomposition of $CaCO_3$. The weight loss of 8.9 wt.% in the temperature range of 150–300 °C is due to the decomposition of the polymer (Fig. S25, Supplementary Material). Wang and co-workers [24] employed carboxylate-based polyesters possessing a degree of carboxylation of 71.3%, which is close to the corresponding value (70%) of hb oligomers employed in our study. These authors found that 8.7 wt.% of polymer is attached to the single spherical vaterite particles (with phase purity of 96%) by direct mixing of precursor solutions. However, the calcium and carbonate concentrations reported in this study (0.025 M) were much lower than those used in our investigations (0.5 M) and thus hardly comparable. In contrast, carboxylate-terminated PAMAM dendrimers [17] showed approximately 30 wt.% of polymer bound to vaterite particles, which were obtained by direct mixing of stock solutions. On the other hand, You et al. [20] reported pure calcite formation by slow vapor diffusion using COO-terminated hyperbranched polyglycidol. These significant differences in the obtained polymorph of $CaCO_3$ are due to the employed crystallization method, which influences the nucleation and growth of $CaCO_3$. For all these similarly branched polymers functionalized with carboxylate groups, direct mixing of precursor solutions led to vaterite, slow vapor diffusion led to the thermodynamically more stable product calcite, and spray-coating in our case led to a mixture of both polymorphs showing that COO-terminated *hb*-PG could – at least partially – initiate vaterite nucleation and growth under these conditions. If compared to SO_4-terminated *hb*-PG, carboxylated polyglycidol seems less suitable for stabilizing a high level of supersaturation of $CaCO_3$, and it seems to act less selective in directing the formation of a particular $CaCO_3$ polymorph. The highest amount of vaterite that could be obtained in our experiments employing COO-terminated *hb*-PG was 45%. Even though no formation of a single pure $CaCO_3$ phase was achieved, these results show that dense calcite–vaterite composites can be effectively prepared in the presence of COO-terminated *hb*-PG with spray technique.

3.4. Spray-coating preparation of calcite composites in the presence of OPO_3HPhOH-terminated hb-PG

Compared to carboxylate functionalized polymers, polymeric additives bearing phosphate monoester groups have so far rarely been employed as soluble additives in $CaCO_3$ crystallization. Phosphate groups were identified as good modifying groups due to the low solubility product of calcium phosphate [44], and it was shown that they can strongly interact with the surface of calcium minerals [16,45].

The morphology of the composite obtained with hyperbranched polyglycidol functionalized with phosphate monoester groups (OPO_3HPhOH-terminated *hb*-PG) in our experiments differs considerably from the film morphologies obtained by the other functionalized hyperbranched polyglycidols. Whereas the sulfate functionalized polyglycidol showed distinct influence on the $CaCO_3$ morphology and preferred vaterite formation, the phosphate monoester functionalized polyglycidol led exclusively to calcite formation with a strong impact on morphology. The crystal phase of the polycrystalline $CaCO_3$ thin film made in the presence of OPO_3HPhOH-terminated *hb*-PG was characterized first by XRPD, and quantitative phase analysis showed that pure calcite is present (Figs. S26 and S27, Supplementary Material). The calcite thin film demonstrated preferred orientation along the [001] direction. The Raman and FT-IR spectra confirm calcite formation indicated by an absorption band at 714 cm^{-1} (v_4) (Figs. S28 and S29, Supplementary Material). Two additional bands at 1090 cm^{-1} and at 1010 cm^{-1} were found in the FT-IR spectrum, which corresponds to the P–O–C bending modes of the phosphate monoester groups

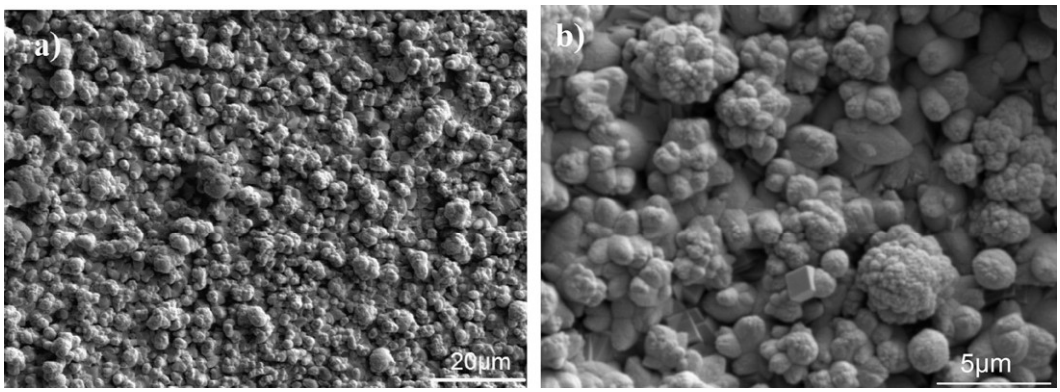

Fig. 4. SEM micrographs showing morphological characteristics of the calcite–vaterite composite obtained by spray technique in the presence of COO-terminated *hb*-PG. (a) Low magnification and (b) high magnification.

from the polymer, since no infrared active band occurs for calcite in this region. By EDX analysis, a small amount of phosphorous bound to the composite (Fig. S30, Supplementary Material) was found. Thus, the presence of polymer bound to the calcite was proved by EDX and FT-IR. Thermogravimetric analysis (Fig. S31, Supplementary Material) of the composite was carried out to determine the amount of incorporated polymer within the composite. The first weight loss of 13.1% occurs upon heating to 300 °C and corresponds to the decomposition of the polymer, whereas the second weight loss of 38.2% occurs from 700 °C on, which is due to $CaCO_3$ decomposition. The adsorbed OPO_3 HPhOH-terminated *hb*-PG showed pronounced morphological impact on the $CaCO_3$ composite. Suppressing the regular rhombohedral growth of typical calcite crystals, rosette-like structures are observed, which show a layered and confluent intergrowth of calcite platelets, as revealed by SEM images (Fig. 5a and b). The XRPD analysis shows that this composite is constructed of small subunits with a primary particle size of 250 nm, as revealed by the width of the (104) reflection. Employing a profilometer, it was found that an essentially uniform film thickness in the narrow range of 3.3–3.5 μm is characteristic for this composite. Noteworthy is that when the oligomer concentration was decreased by nearly 10 times, that is, from 10 mg/mL to 1.23 mg/mL, even at this low concentration a composite was obtained, although the morphology was changed. SEM micrographs of the obtained composite, which contains larger crystal specimen and a rough surface texture, are shown in Fig. 5c and d. Two different morphologies can be clearly seen: rhombohedral particles with sharp edges and smooth surface areas showing intergrown spherical particles. The single polymorph accomplished in this second composite was calcite as well, as proved by XRPD (data not shown). The single crystalline domains were estimated to have a size of approx. 205 nm as determined from the (104) reflection. An EDX measurement detected a small amount of phosphorous bound to the composite as well (Fig. S32, Supplementary Material). Despite the low degree of phosphorylation of only 26% and the low polymer concentration, OPO_3HPhOH-terminated *hb*-PG demonstrates a very strong influence on $CaCO_3$ morphology.

As it was mentioned above, phosphate groups generally show high association constants with Ca^{2+} ions and strong adsorption to the surface of calcium carbonate crystals [16]. In a series of publications [16], it was reported that block-copolymers with different degrees of phosphorylation and applied at different concentrations are able to modify the $CaCO_3$ crystal morphology, yielding either pure vaterite or a mixture with calcite.

The chosen crystallization methods were Kitano method and double-jet technique with stirring. It was also reported that the higher the degree of phosphorylation (40%), the lower the stabilization efficiency per functional group, suggesting that only a certain fraction of phosphate groups will interact and thus influence $CaCO_3$ formation [16]. In our experiments using OPO_3HPhOH-terminated *hb*-PG (26% degree of phosphorylation), two different concentrations were tested, leading to two different calcite morphologies. Our results are in a good agreement with the above mentioned results relating to the effect of different polymer concentration on $CaCO_3$ morphologies. An interconnection between the $CaCO_3$ aggregates present in the calcite film was obtained even at the lowest polymer concentration level. Mann et al. [46] reported that ester derivatives of orthophosphate showed a marked reduction in the morphological effects exerted on $CaCO_3$ as the R group increased in size and hydrophobicity (H > butyl > phenyl > naphthyl). As a possible explanation, different stereochemical arrangements of phosphate groups with the inorganic crystal faces were discussed, which seem to depend strongly on the chemical nature of the

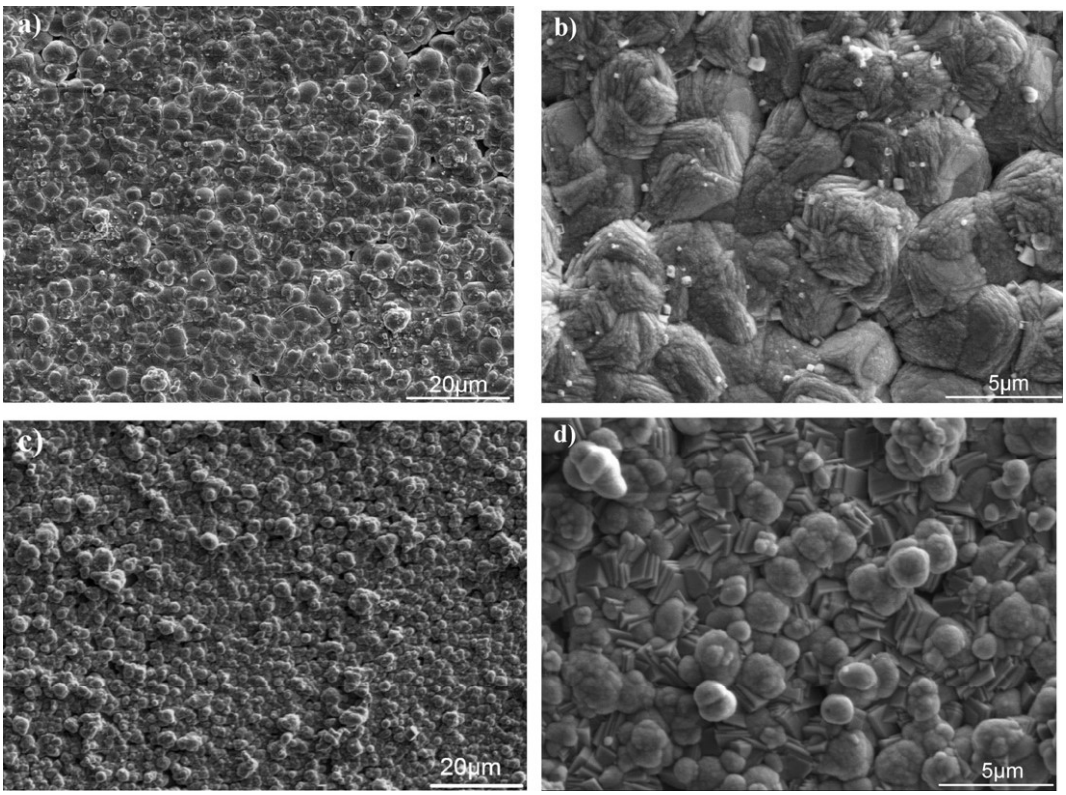

Fig. 5. SEM micrographs showing morphological characteristics of calcite composite obtained by spray technique in the presence of OPO_3HPhOH-terminated *hb*-PG. (a and b) low and high magnification, respectively, in the presence of 20 mM OPO_3HPhOH-terminated *hb*-PG; (c and d) low and high magnification, respectively, in the presence of 2.5 mM OPO_3HPhOH-terminated *hb*-PG.

phosphate ester residue R. Crystal morphologies similar to ours were obtained by using phenyl phosphoester, which led to well defined crystals, showing a curved cross-section with a smooth surface.

3.5. Mechanical properties

Mechanical properties of calcite composite thin films produced by the novel spray technique employing OPO_3HPhOH-terminated *hb*-PG were investigated and compared to neat calcite. The mechanical tests were performed in two ways: by simple pre-tests (scratch resistance) and by nanoindentation. Due to the relatively low height of the thin films, nanoindentation was chosen for measuring the mechanical properties, since small scale volumes (e.g., thin films, nanowires, nanotubes, fibers, small particles, electronics) are difficult to probe using conventional techniques. As an almost non-destructive technique, nanoindentation thus allowed us to measure the as-prepared film without removing it from the substrate [47,30].

The samples prepared in the presence of SO_4-terminated *hb*-PG and COO-terminated *hb*-PG show a low mechanical stability, since they were not scratch resistance against a finger nail (indicating a scratch resistance lower than 2 on the Mohs scale, and thus lower than neat $CaCO_3$) [48,49]. In contrary, the polycrystalline $CaCO_3$ thin films prepared in the presence of OPO_3HPhOH-terminated *hb*-PG at different concentrations showed scratch resistance against a finger nail and thus were further investigated by nanoindentation. Two calcite composite coatings were investigated, which were prepared in the presence of 2.5 mM or 20 mM OPO_3HPhOH-terminated *hb*-PG, respectively. Nanoindentation was used to investigate the reduced Young's modulus (E_R) and hardness (H) at a constant load of 7.5 mN. These mechanical properties were determined from the load–displacement curves using the Oliver–Pharr method [30]. Representative examples for the load–displacement curves are given in Fig. 6, and the resulting average values resulting for E_R and H are presented in Table 1. The obtained E_R and H for neat calcite are $E_R = 81.3 \pm 3.3$ GPa and $H = 2.4 \pm 0.1$ GPa, respectively, which are in good agreement with values reported in the literature (reported values are in the range of $H = 2.2–3.0$ GPa and $E = 73.5–85$ GPa) [49].

The values of E_R and H of the calcite composites are depending on the OPO_3HPhOH-terminated *hb*-PG concentration used during the spray process. The composite prepared in the presence of

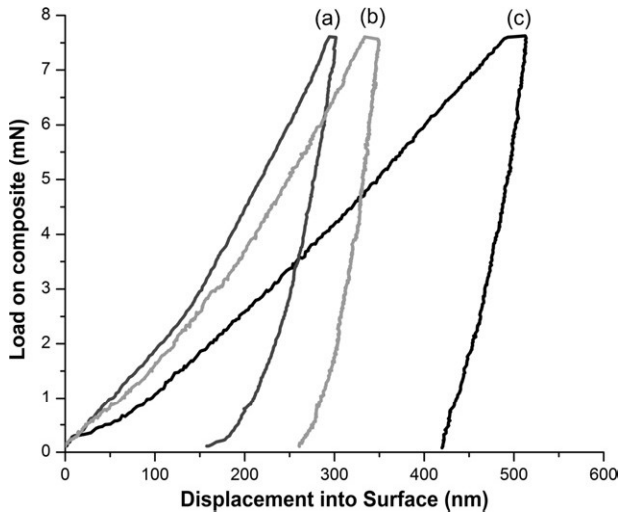

Fig. 6. Representative load–displacement curves for nanoindentation experiments performed with a load of 7.5 mN on (a) calcite composite made in the presence of 20 mM OPO_3HPhOH-terminated *hb*-PG; (b) neat calcite; (c) calcite composite made in the presence of 2.5 mM OPO_3HPhOH-terminated *hb*-PG.

Table 1
Mean mechanical properties, modulus (E_R) and hardness (H) of calcite composite in the presence of OPO_3HPhOH-terminated *hb*-PG formed by spray process and control sample of natural calcite.

Sample	Modulus (E_R) (GPa)	Hardness (H) (GPa)
Composite (a)	55.1 ± 20.4	3.0 ± 1.1
Neat calcite (b)	80.3 ± 3.7	2.4 ± 0.1
Composite (c)	43.1 ± 20.1	1.1 ± 0.9

Composite (a): calcite composite in the presence of 20 mM OPO_3HPhOH-terminated *hb*-PG; composite (c): calcite composite in the presence of 2.5 mM OPO_3HPhOH-terminated *hb*-PG.

20 mM OPO_3HPhOH-terminated *hb*-PG (composite (a) shows an increase in hardness by 20% when compared to neat calcite, whereas the Young's modulus is slightly decreased (Table 1). On the other hand, by decreasing the oligomer concentration to 2.5 mM (composite (c), both of these values are decreased below E_R and H of neat calcite. The reduction (or only slight increase in the hardness in one case) in the mechanical properties in comparison with neat calcite seems to be due to the fact that calcite as a hard particle is embedded in a relatively soft polymer matrix. In many cases, it has been observed experimentally that the hardness of a composite is the average obtained by a simple "rule of mixture" [50,51] from both hardness values of the constituting pure components.

Exceptions of this "rule of mixture" are found when the size of the particles embedded in the soft matrix are in the order of a few nanometers, and when a highly ordered structure is present [51]. Accordingly, calcite composite (a), which was prepared in the presence of higher oligomer concentration compared to calcite composite (c), showed the highest value of hardness in contrast to neat calcite and calcite composite (c). This increase in hardness seems to be due the more regular morphology and the intimate packing of the mineral particles (Fig. 5b), contrasting calcite composite (c), which shows two different kinds of morphologies (Fig. 5d). In conclusion, whereas the spray technique is generally suitable for the preparation of dense composite thin films, there is still a huge potential to increase the mechanical properties by developing more sophisticated polymer molecules. In order to improve the hardness of the coatings, the polymer should stronger adsorb on the $CaCO_3$ crystallites to guarantee a more intimate contact and produce smaller crystallites in the resulting composite coating.

4. Conclusions

Using spray technique, the preparation of dense $CaCO_3$ hybrid film in combination with hyperbranched polyglycidol comprising different functional groups (phosphate monoester, sulfate and carboxylate groups) is described for the first time. The spray technique seems to be the most promising method for the huge-scale preparation of biologically inspired $CaCO_3$ composite thin films, since large surface areas can be covered by an industrially established set-up at high deposition rates, in contrast to other crystallization methods established in this field. Via spray-coating technique, $CaCO_3$ composites with selective control of the $CaCO_3$ polymorph and crystal morphology were prepared. SO_4-terminated *hb*-PG as additive in the spray-coating deposition of thin films exclusively led to formation of vaterite. This coating shows long-term stability: the polymorph remained unchanged for an exceptional period of more than 9 months. In contrast, the $CaCO_3$ composite produced in the presence of COO-terminated *hb*-PG shows the formation of equal quantities of calcite and vaterite. The effect of the phosphate monoester group led to the formation of a very dense calcite composite with a constant film thickness

ranging from 3.3 to 3.5 μm in height. The results from mechanical investigations show that, depending on the oligomer employed, the *E*-modules and hardness of the composite thin films exceed those measured for neat calcite under identical experimental conditions, albeit the overall mechanical performance will require further optimization of polymer structure and processing conditions.

Acknowledgments

Financial support by the DFG (DFG Materials Network, grant VO 829/4-1) is gratefully acknowledged. We thank Dr. P. Reuter (University Ulm) for capturing SEM images and EDX spectra, Chem.-Ing. A. Kalytta-Mewes for assistance with the mechanical properties and Dr. M. Grzywa for performing Rietveld refinements.

References

[1] (a) M.F. Ashby, L.J. Gibson, U. Wegst, R. Olive, Proc. Roy. Soc. Lond. A 450 (1995) 123;
(b) M. Fritz, D.E. Morse, J. Microsc. 212 (2003) 280;
(c) P. Calvert, P. Rieke, Chem. Mater. 8 (1996) 1715.
[2] (a) H.A. Lowenstam, S. Weiner, On Biomineralization, Oxford University Press, New York, 1989;
(b) L. Addadi, S. Weiner, Angew. Chem. Int. Ed. 31 (1992) 153;
(c) S. Weiner, L. Addadi, J. Mater. Chem. 7 (1997) 689;
(d) S.L. Lee, A. Veis, T. Glonek, Biochemistry 16 (1977) 2971.
[3] (a) A.P. Jackson, J.F.V. Vincent, R.M. Turner, Proc. Roy. Soc. Lond. B 234 (1988) 415;
(b) A.P. Jackson, J.F.V. Vincent, R.M. Turner, Compos. Sci. Technol. 36 (1989) 255;
(c) A.G. Evans, Z. Suo, R.Z. Wang, I.A. Aksay, M.Y. He, J.W. Hutchinson, J. Mater. Res. 16 (2001) 2475.
[4] S. Kamat, X. Su, R. Ballarini, A.H. Heuer, Nature 405 (2000) 1036.
[5] (a) A. Perez-Huerta, M. Cusack, W. Zhu, J. England, J. Hughes, J. Roy. Soc. Interface 4 (2007) 33;
(b) S. Zügner, K. Marquardt, I. Zimmermann, Eur. J. Pharm. Biopharm. 62 (2006) 194;
(c) A. Williams, The evolution of the shell structure of articulate brachiopods, Special Papers in Palaeontology, 2, The Palaeontological Association Press, London, UK, 1968.
[6] (a) S. Stupp, P.V. Braun, Science 277 (1997) 1242;
(b) S. Mann, G. Ozin, Nature 382 (1996) 313;
(c) A. Lin, M.A. Meyers, Mater. Sci. Eng. A 390 (2005) 27;
(d) Y. Oaki, H. Imai, Angew. Chem. 117 (2005) 6729.
[7] R. Menig, M.H. Meyers, M.A. Meyers, K.S. Vecchio, Acta Mater. 48 (2000) 2383.
[8] (a) Y. Oaki, H. Imai, Angew. Chem. Int. Ed. 44 (2005) 6571;
(b) R. Chen, C.A. Wang, Y. Huang, H.R. Le, Mater. Sci. Eng. C 28 (2008) 218;
(c) Z. Tang, N.A. Kotov, S. Magonov, B. Ozturk, Nat. Mater. 2 (2003) 413.
[9] (a) T. Kato, A. Sugaware, N. Hosoda, Adv. Mater. 14 (2002) 869;
(b) A. Sugawara, T. Kato, Chem. Commun. (2000) 487;
(c) L. Addadi, J. Moradian, E. Shay, N.G. Maroudas, S. Weiner, Proc. Natl. Acad. Sci. USA 84 (1987) 2732.
[10] (a) H. Wei, N. Ma, F. Shi, Z. Wang, X. Zhang, Chem. Mater. 19 (2007) 1974;
(b) P. Podsiadlo, S. Paternel, J.M. Rouillard, Z. Zhang, J. Lee, J.M. Lee, E. Gulari, N. Kotov, Langmuir 21 (2005) 11915.
[11] C. Wang, B. Long, W. Lin, Y. Huang, J. Sun, J. Mater. Res. 23 (2008) 1706.
[12] D. Volkmer, M. Harms, L. Gower, A. Ziegler, Angew. Chem. Int. Ed. 44 (2005) 639.
[13] H. Cölfen, L. Qi, Chem. – Eur. J. 7 (2001) 106.
[14] (a) Q. Yu, H.D. Ou, R.Q. Song, A.W. Xu, J. Cryst. Growth 286 (2006) 178;
(b) H. Yu, M. Lei, B. Cheng, X.J. Zhao, J. Solid State Chem. 177 (2004) 681.
[15] (a) A. Jayaraman, G. Subrambramyam, S. Sindhu, P.K. Ajikumar, S. Valiyaveettil, Cryst. Growth Des. 7 (2007) 142;
(b) H. Cölfen, M. Antonietti, Langmuir 14 (1998) 582;
(c) K. Naka, Y. Tanaka, Y. Chujo, Y. Ito, Chem. Commun. (1999) 1931.
[16] (a) K. Kaluzynski, J. Pretula, G. Lapienis, M. Basko, Z. Bartczak, A. Dworak, S. Penczek, J. Polym. Sci. Part A: Polym. Chem. 39 (2001) 955;
(b) K. Sawada, N. Abdel-Aal, H. Sekino, K. Satoh, Dalton Trans. 3 (2003) 342;
(c) J. Rodloff, M. Antonietti, H. Cölfen, J. Pretula, K. Kaluzynski, S. Penczek, Macromol. Chem. Phys. 203 (2002) 627.
[17] (a) K. Naka, Top. Curr. Chem. 228 (2003) 141;
(b) D.K. Keum, K. Naka, Y. Chujo, Bull. Chem. Soc. Jpn. 76 (2003) 1687;
(c) K. Naka, Y. Tanaka, Y. Chujo, Langmuir 18 (2002) 3655.
[18] C. Gao, D. Yan, Prog. Polym. Sci. 29 (2004) 183.
[19] (a) R. Wilson, B.J. Van Schie, D. Howes, Food Chem. Toxicol. 36 (1998) 711;
(b) R.K. Kainthan, D.E. Brooks, Biomaterials 28 (2007) 4779.
[20] G. Wang, L. Li, J. Lan, L. Chen, J. You, J. Mater. Chem. 18 (2008) 2789.
[21] (a) M.Q. Slagt, S.E. Stiriba, H. Kautz, R.J.M. Klein Gebbink, H. Frey, G. van Koten, Macromolecules 35 (2002) 5734;
(b) S.E. Stiriba, H. Kautz, H. Frey, J. Am. Chem. Soc. 124 (2002) 9698;
(c) S.C. Zimmerman, J.R. Quinn, E. Burakowska, R. Haag, Angew. Chem. Int. Ed. 46 (2007) 8164;
(d) H. Türk, A. Shukla, P.C.A. Rodrigues, H. Rehage, R. Haag, Chem.-Eur. J. 13 (2007) 4187.
[22] (a) D.H. Bolton, K.L. Wooley, J. Polym Sci. Part A: Polym. Chem. 4 (2002) 823;
(b) M. Jikei, M. Kakimoto, Prog. Polym. Sci. 26 (2001) 1233;
(c) C.R. Yates, W. Hayes, Eur. Polym. J. 40 (2004) 1257.
[23] M. Balz, E. Barriau, V. Istratov, H. Frey, W. Tremel, Langmuir 21 (2005) 3987.
[24] Q. Meng, D. Chen, L. Yue, J. Fang, H. Zhao, L. Wang, Macromol. Chem. Phys. 208 (2007) 474.
[25] W. Dong, H. Cheng, Y. Yao, Y. Zhou, G. Tong, D. Yan, Y. Lai, W. Li, Langmuir 27 (2011) 366.
[26] (a) Y. Kitano, K. Park, D.W. Hood, J. Geophys. Res. 67 (1962) 4873;
(b) R.J. Park, F.C. Meldrum, Adv. Mater. 14 (2002) 1167.
[27] H. Gong, M. Pluntke, O. Marti, P. Walther, L. Gower, H. Cölfen, D. Volkmer, Colloids Surf. A 354 (2010) 279.
[28] EP 2029675 A1, EP 1835053 B1, US 7361324 B2, US 07544496, US 07514249, US 07514248, ADA438246.
[29] (a) A.V. Bers, G.S. Prendergast, C.M. Zürn, L. Hansson, R.M. Head, J.C. Thomason, Biol. Lett. 2 (2006) 88;
(b) EP 1 835 053 B1.
[30] W.C. Oliver, G.M. Pharr, J. Mater. Res. 7 (1992) 1564.
[31] F. Manoli, E. Dalas, J. Cryst. Growth 217 (2000) 416.
[32] K. Naka, S.-C. Huang, Y. Chujo, Langmuir 22 (2006) 7760.
[33] A. López-Macipe, J. Gómez-Morales, R. Rodríguez-Clemente, J. Cryst. Growth 166 (1996) 1015.
[34] (a) N. Hosoda, A. Sugawara, T. Kato, Macromolecules 36 (2003) 6449;
(b) T.J. Han, X. Xu, D.H. Kim, K. Cho, Chem. Mater. 17 (2005) 136;
(c) N. Wada, S. Suda, K. Kanamura, T. Umegaki, J. Colloid Interf. Sci. 279 (2004) 167.
[35] (a) M.M. Tlili, M. Ben Amor, C. Gabrielli, S. Joiret, J. Maurin, P. Rousseau, J. Raman Spectrosc. 33 (2001) 10;
(b) M. Faatz, F. Gröhn, G. Wegner, Adv. Mater. 16 (2004) 996;
(c) S. Raz, S. Weiner, L. Addadi, Adv. Mater. 12 (2000) 38.
[36] International Centre for Diffraction Data (ICDD), PDF-4+, 2006.
[37] (a) ICSD-Inorganic Crystal Structure Database, Version 1.4.6, 2009–2, Fachinformationszentrum, Karlsruhe, Germany.;
(b) V. Petricek, M. Dusek, L. Palatinus, Jana 2000, The Crystallographic Computing System, Institute of Physics, Praha, Czech Republic, 2000.
[38] W.A. Dollase, J. Appl. Crystallogr. 19 (1986) 267.
[39] (a) J. Rieger, J. Thieme, C. Schmidt, Langmuir 16 (2000) 8300;
(b) J. Rieger, T. Frechen, G. Cox, W. Heckmann, C. Schmidt, J. Thieme, Faraday Discuss. 136 (2007) 265.
[40] (a) F.C. Nart, T. Iwasita, J. Electroanal. Chem. 308 (1991) 277;
(b) S.D. Ross, in: V.C. Farmer (Ed.), The infrared spectra of mineral, Miner. Soc. Monogr. 1974, p. 423.;
(c) K. Omori, Miner. J. 5 (1986) 334;
(d) L.A. Guirguis, TIZ-Fachberichte 111 (1987) 339.
[41] P. Scherrer, Nachr. Ges. Wiss. Göttingen 2 (1918) 96.
[42] (a) B. Barbarray, J.P. Contour, G. Mouvier, Atmos. Environ. 11 (1977) 351;
(b) C.R. Brundle, A.F. Carley, Faraday Discuss. Chem. Soc. 60 (1975) 51;
(c) D. Briggs, M.P. Seah, Practical Surface Analysis by Auger and X-ray Photoelectron Spectroscopy, Wiley, Chichester, 1983. p. 283.
[43] D.R. Bain, M.C. Café, I.D. Robb, P.A. Williams, J. Colloid Interf. Sci. 88 (1982) 467.
[44] O. Söhnel, J. Garside, Precipitation: Basic Principles and Industrial Applications, Butterworth, Heinemann, Oxford, 1992.
[45] (a) T. Wang, G. Rother, H. Cölfen, Macromol. Chem. Phys. 206 (2005) 1619;
(b) A.-W. Xu, Q. Yu, W.-F. Dong, M. Antonietti, H. Cölfen, Adv. Mater. 17 (2005) 2217.
[46] J.M. Didymus, P. Oliver, S. Mann, A.L. Devries, P.V. Hauschka, P. Westbroek, J. Chem. Soc. Faraday Trans. 89 (1993) 2891.
[47] Rashid K. Abu Al-Rub, Mech. Mater. 39 (2007) 787.
[48] American Federation of Mineralogical societies: Mohs Scale of Mineral Hardness.
[49] (a) M.E. Broz, R.F. Cook, D.L. Whitney, Am. Mineral. 91 (2006) 135;
(b) Y.R. Ma, S.R. Cohen, L. Addadi, S. Weiner, Adv. Mater. 20 (2008) 1555.
[50] (a) R. Warren, Ceramic–Matrix Composites, Chapman and Hall, Inc., New York, 1992;
(b) H.S. Kim, Mater. Sci. Eng. A 289 (2000) 30;
(c) T.W. Clyne, D.W. Hull, An Introduction to Composite Materials, second ed., Cambridge University Press, New York, 1996.
[51] J.A. Schwarz, C.I. Contescu, K. Putyera (Eds.), Encyclopedia of Nanoscience and Nanotechnology, vol. 5, Marcel Dekker Inc., New York, 2004, p. 4381.